# Synthesis and characterization of squaramide-based supramolecular polymers

Lauria, F.

# CHAPTER 4

# Understanding the self-assembly of tripodal squaramide-based monomers through structural substitution

## 4.1 Abstract

The chemical structure of a supramolecular monomer and the environment it is placed in plays a critical role on its self-assembly and formation of supramolecular polymers. However, the structure and the properties of the formed polymers are difficult to predict starting from the monomers *a priori*. We earlier demonstrated that tripodal squaramide-based monomers self-assemble into long, flexible supramolecular polymers and gel-phase materials above a critical concentration in water. Modulation of the hydrophobic domains of the monomer, had a lesser impact on the formation of fibrillar aggregates, however gel-phase materials were only formed for monomers with a particular hydrophilic-hydrophobic ratio. In this chapter, I take a step further in designing a small library of squaramide-based monomers to delineate the structural modifications that are necessary to trigger the formation of fibrillar aggregates. Since self-assembly of the monomer in aqueous solution requires a synergy between hydrophobic and hydrogen bonding interactions, structural modifications to the monomer involving either or both of these interactions were examined. In particular, a family of squaramide monomers were designed to consider the effect of carbamate bond, ether linkage, decreasing the number of squaramide units from three to two and varying the number of tetraethylene glycol moieties. Substitution of carbamate linkage with an ether bond results in the formation of a 4-fold less stiff hydrogel relative to the native tripodal squaramide monomer. Reduction in the number of squaramide moieties resulted in the lack of monomer gelation at similar condition, but the formation of supramolecular polymers was still observed. Moreover, replacing one hydrophobic domain resulted in the solubilization of the monomer and the loss of the formed supramolecular polymers, further emphasizing the importance of the synergy of all monomer features on supramolecular polymerization and hydrogel formation.

## 4.2 Introduction

Supramolecular polymers have sparked much interest for a broad range of applications in healthcare due to their unique properties that arise from the inherent dynamic character of the interactions that hold them together.[1,2] Accessible to this class of polymers are properties such as tunability, responsiveness, modularity, recyclability, and biomimicry.[3] Consequently, they are being examined for several application areas such as tissue engineering,[4] regenerative medicine,[5] drug delivery[6] and as mimics of extracellular matrix for 3D cell culture.[7, 8] Two classes of materials are employed in this area, those consisting of polymers with modules that engage in molecular recognition and those that self-assemble through stacking of monomers under physiological conditions.[3] In both of these classes, gel-phase materials can be formed when applied above a critical concentration depending on their molecular structure. Hence, gaining insight into the features of the monomers that drive supramolecular polymerization and their effect on the formation of water-based materials is critical to their application in the abovementioned areas.

In the design of a supramolecular monomer for polymerization, non-covalent interactions such as hydrogen bonding, π-π, electrostatic and hydrophobic interactions are strategically positioned taking into account the microenvironment of the selected interaction (e.g. with respect to the solvent) and combination of interactions. However, rational design of such monomers and prediction of the final self-assemblies remains challenging, especially in water that can have a potent effect on the self-assembly pathway of the aggregates. The hydrophobic effect[9] drives the self-assembly of amphiphile molecules in combination with other directional interactions.[10] Hydrogen bonding on supramolecular synthons such as 1,3,5-benzenetricarboxamide (BTAs),[11] peptides,[12,13] and ureidopyrimidones[14-16] have been employed in the monomer design to prepare supramolecular polymers and gel-phase materials in water.

Of the examined monomer geometries, tripodal and $C_3$-symmetric cores, have have been widely applied in the construction of supramolecular materials.[17-19] BTAs represent one of the most studied scaffolds in supramolecular chemistry.[11] The self-assembly of BTAs into supramolecular polymers in organic solvent relies on a combination of π-π and hydrogen bonds interactions from the amide groups with a high degree of cooperativity.[11,20,21] Reduction of the monomer to a $C_2$-symmetry resulted in a ten-fold lower

cooperativity as compared to $C_3$ symmetry in methylcyclohexane (MCH). The consequence of reduced cooperativity results in a decreased size and morphological change of the resulting aggregates.[22] When oligo(ethylene glycol) chains are added to the periphery of BTAs-based monomer, possibilities to use this synthon for self-assembly in water are unlocked.[23,24] In this study, the minimum aliphatic chain length required for the self-assembly in water, but also the inclusion of stereogenic centers on chiral handedness of the final aggregates were disclosed.[23,24] Besenius, Meijer and coworkers further examined the effect of installing periphery units that provide function on the BTA monomer such as Gd(III)–DTPA (diethylene triaminepentaacetic acid) introducing electrostatic effects into the self-assembly and potential for imaging.[25]

Cyclohexane-based $C_3$-symmetric 1,3,5-cyclohexane trisamide (CTA)-cores have also been examined to prepare materials in water, showing potent self-assembly and gelation properties.[26-28] van Esch and coworkers prepared phenylalanine derivatives with a CTA core containing different stereogenic centers and demonstrated their effect on hydrogelation.[26] Moreover, Eelkema and coworkers investigated the potential to tune the morphology of the self-assembled CTAs by modulating the monomer structure.[29] In particular, the gelator was designed with two segments: a CTA core functionalized with three phenylalanines substituted with tetraethylene glycol chains and one with a hydrophobic aliphatic segment. When a chaperone was added, the self-assembly properties of each individual segments could be controlled resulting in a switch in morphology from twisted tapes to nanofibers and the loss of gel phase properties. On the other hand, addition of HFIP, a good solvent for the monomer and a hydrogen bond disrupting solvent resulted in the formation of micellar aggregates. While significant progress in understanding the effect of certain structural modifications on the self-assembly behaviour of $C_3$-symmetric amphiphiles in organic solvents and water has been made in these studies, most examples have been limited to the use of amides as the ditopic hydrogen bonding unit.

Squaramides are ditopic hydrogen bonding synthons consisting of a cyclobutenedione ring that have applied in the areas of catalysis, bioconjugation, as ion receptors and in the design of supramolecular materials due to their ability to form strong hydrogen bonds.[30-35] We recently reported a tripodal squaramide-based monomer that self-assembles into supramolecular polymers and gel-phase materials in water.[36] Specifically, the squaramide synthon was incorporated into the hydrophobic domain and surrounded with

tetraehtylene glycol chains. Supramolecular monomers were designed with different aliphatic chain lengths ranging from 6-12 methylene units, but only those with 8 and 10 methylenes resulted in the formation of hydrogels highlighting the importance of the hydrophilic-hydrophobic balance on the self-assembly of the monomers. Inspired by these results, we were interested to further understand the self-assembly scope of this monomer, examining non-uniform changes to its geometry and hydrophobic content, as well as the number of squaramides and presence of the carbamate moiety. Herein a library of tripodal squaramide-based monomers was reported and the effect of these structural substitutions on their self-assembly into supramolecular polymers and hydrogels was examined.

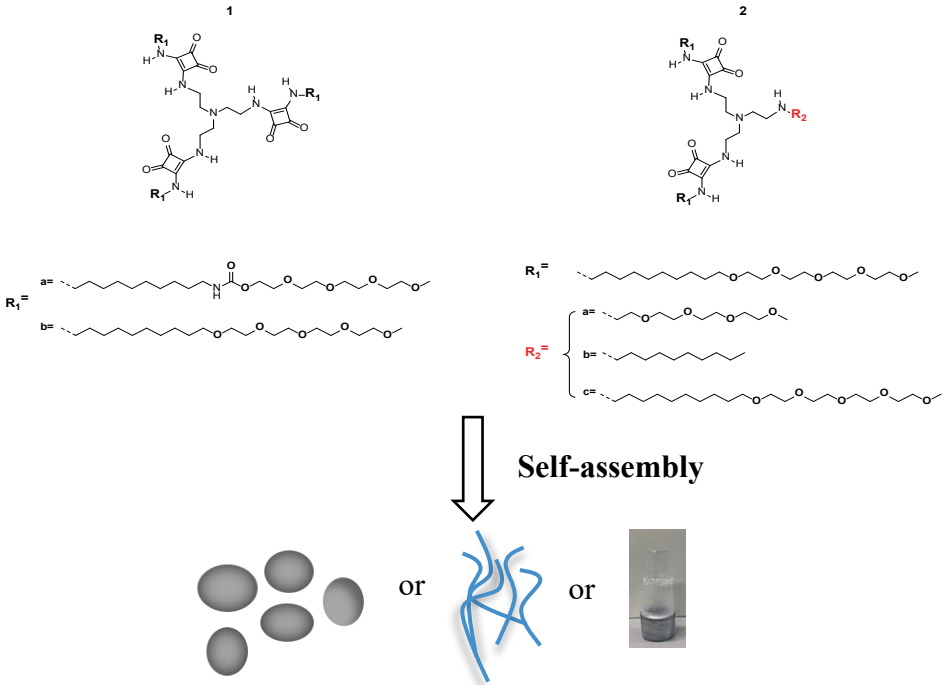


**Figure 4.1** Squaramide-based tripodal supramolecular monomers used in this study and the examination of their self-assembly into supramolecular polymers and gel-phase materials.

## 4.3 Results and discussions

In order to better understand the features of the tripodal squaramide-based monomer (**1a**) that enables it to form supramolecular hydrogel, a small library of monomers were prepared with various structural modifications. The molecular structure of the monomer contains three squaramide moieties, C10 aliphatic and tetraethylene glycol chains. The combination of these features drives their self-assembly into supramolecular polymers in water and thus, modifications that would impact this process were examined.[37] Hence, the effect of structural modifications involving either or both of these interactions simultaneously on the monomer were explored. In our earlier design, a carbamate moiety was used to connect the aliphatic spacers to the oligoethyelene glycol chains because of its synthetic facility. However, to understand the effect of the carbamate bonds on supramolecular polymerization of the squaramide monomers, this linkage was exchanged for an ether in all molecules of the library (**1b** and **2a-c**).

Ether linkages were introduced into squaramide-based amphiphile (**6**) according to an earlier report by Mejier[38] and coworkers (**scheme 1)**. Tetraethylene glycol monomethyl ether was coupled with the C10 aliphatic spacer in presence of NaH and 1,10-dibromodecane. The obtained amphiphile containing a halide (**3**) was converted in primary amine by the Gabriel synthesis in presence of potassium phthalimide and subsequent use of hydrazine monohydrate. The primary amine on the amphiphile (**5**) was subsequently coupled with 3,4-dibutoxy-3-cyclobutene-1,2-dione to obtain the squaramide-based amphiphile (**6**). The monomer **1b** was synthesized as reported previously by our group[36] with the coupling of tris(2-aminoethyl amine) (TREN) core in presence of an excess of squaramide amphiphile **(6)**.

The effect of reducing the number of squaramide moieties and modifying the hydrophilic-hydrophobic ratio of the monomer were examined in a second group of monomers. Two of the tripodal arms were outfitted with the squaramide amphiphiles and third one was coupled with either an oligoethylene glycol **2a,** ($\omega_{TEG}$ = 0.55), a chain short alkyl chain **2b,** ($\omega_{TEG}$ = 0.53), or an alkyl and oligoethylene glycol **2c,** ($\omega_{TEG}$ = 0.46) chain attached directly to the nitrogen of the monomer core. As reported in **scheme 1**, the syntheses of **2a-c** were performed starting from the squaramide-based amphiphile (**6**) that was coupled with N,N″-di-Z-diethylenetriamine functionalized with an oligoethylene glycol (**2a),** a short alkyl chain (**2b)** or an alkyl and oligoethylene glycol chain (**2c)** respectively. To prepare N,N″-

di-Z-diethylenetriamine, benzylic alcohol was first activated with 1,1-carbonyldiimidazole (CDI) and coupled to bis(2-aminoethyl)amine in excellent yields (**8**). The N,N″-di-Z-diethylenetriamine core was further reacted with oligoethylene glycol**,** a C10 alkyl chain or an alkyl and oligoethylene glycol chain as reported by Wadas[39] and coworkers. Subsequently, after hydrogenation *in situ* with $Et_3SiH$ on Pd/C to remove the Cbz protecting group, the core was coupled with squaramide-based amphiphile (**6**) to obtain the monomers **2a-c**, in moderate yields.

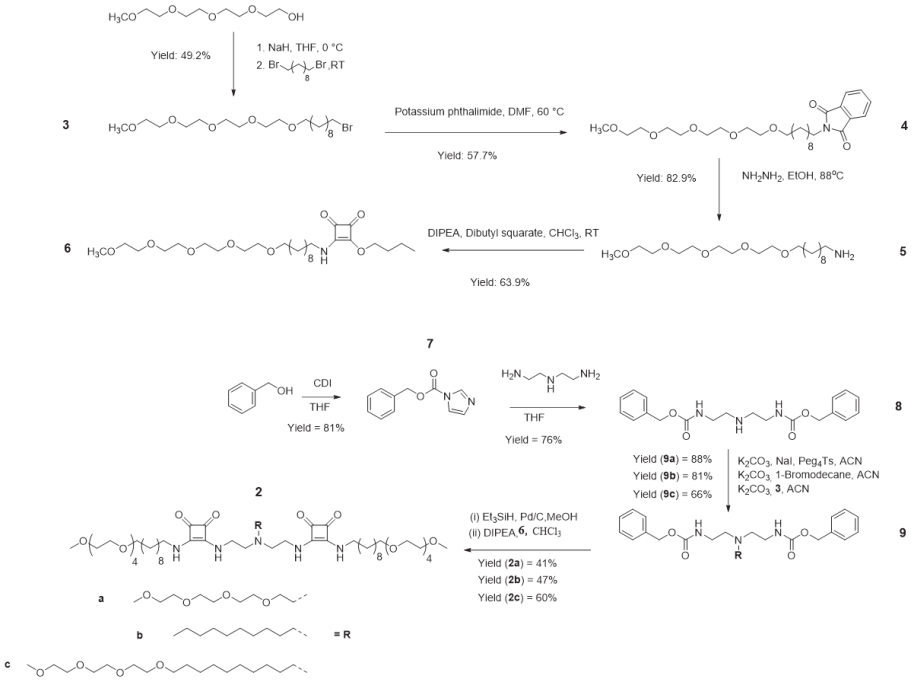


**Synthetic scheme 1**: Synthesis of monomers **2a-c**

Self-assembly of the tripodal squaramide-based monomers **1b** and **2a-c** were first examined at the molecular level in water using UV-vis spectroscopy (**Figure 4.2a)**. In our previous publication[36] the self-assembly of **1a** in water resulted in two absorbance maxima at 255 and 329 nm from the HOMO-LUMO and HOMO-LUMO+1 transitions of the squaramide when self-assembled in a head-to-tail hydrogen bonding arrangement (**1a**). Here, the exchange of the carbamate moiety for ether bonds in the molecular structure of **1b**, resulted in a similar profile to **1a** with the transitions at 255 and 329 nm, respectively. The reduction to two squaramide moieties and one aliphatic spacer replaced with an oligoethylene glycol chain in **2a** resulted in the loss

of these transitions with only one band at 280 nm, consistent with the monomer species and suggestive of a distinct aggregation mode. The addition of an alkyl chain on the third position in **2b** to form a more hydrophobic monomer, gave rise to a UV-vis profile with two bands at 250 and 329 nm as in **1a**, **b,** but with decreased intensity likely due to its poor solubility. The addition of an amphiphile on the third position that lacks a hydrogen bonding group in **2c** results in two maxima at 260 and 329 nm, that are shifted to a lesser degree than either **1a** or **b**, is suggestive of the formation of shorter polymers. Overall, the differences in the shifts of the maxima and their absorbance intensity suggest a variable aggregation patterns of the various squaramide monomers in their respective assemblies.

To further probe the aggregate structures at the molecular level, a fluorescence spectroscopy experiment in the presence of Nile Red dye was performed (**Figure 4.2b**). The Nile Red dye is a hydrophobic probe that increases in fluorescence intensity with a blue-shifted maximum relative to its emission in water when in a hydrophobic environment. Consequently, this dye has been often used to understand the self-assembly of a range of amphiphiles in water.[38,40] The fluorescence spectrum of the Nile Red dye in water displays a low intensity emission band at 640 nm. Monomer **1a** was previously demonstrated to show an intense blue-shifted emission band at 622 nm due to the size of the hydrophobic domains formed on self-assembly in water. The fluorescence spectrum of **1b** displays the same maximum at 622 nm suggesting formation of self-assembled aggregates on par with **1a** as suggested in UV-vis measurements. Because of the increased hydrophilic character of **2a,** the fluorescence emission is comparable to the band in water suggesting a lack of aggregation. Conversely, **2b** containing an aliphatic spacer shows a blue-shifted emission signal at 615 nm of decreased intensity compared to **1b**, whereas **2c** displays an increased fluorescent signal at 622 nm that is consistent with formation of supramolecular aggregates. Thus, the differences in the blue-shifting of the emission maxima and their intensity are consistent with the changes to the hydrophobic and hydrophilic domains of the monomers and their distinct mode of aggregation.

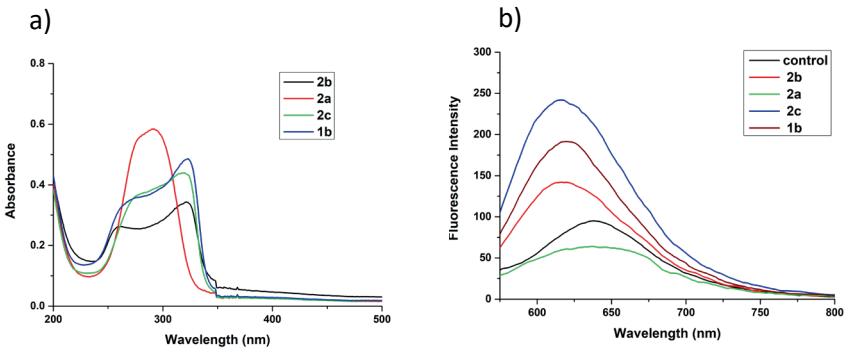


**Figure 4.2** Spectroscopy of tripodal squaramide self-assemblies: (a) UV-vis absorption spectra of **1b, 2a-c** ($c_{SQ}$=15 µM); (b) Fluorescence spectra ($c_{SQ}$=15 µM) of Nile Red dye embedded tripodal molecules **(1b, 2a-c):** ($c_{NileRed}$=0.005 mg/mL, $\lambda_{exc}$ = 550 nm., $\lambda_{em}$ = 570-800 nm), Nile red in MilliQ is used as a control.

Static light scattering (SLS) is a technique used to determine the critical aggregation concentration (CAC) of monomer or the concentration at which a supramolecular polymer is formed. This value is determined from the inflection point of the measured scattering intensity of monomer solutions as a function of concentration.[41] In our previous publication, a concentration-based UV-vis experiment of **1a** displayed the retention of blue- and red shifted bands at even at low concentration ($3.75 \cdot 10^{-6}$ M). Also, the distinct UV-vis profiles of **1b** and **2a** point to the importance of the hydrophobic/hydrophilic balance on monomer self-assembly. Therefore, the critical aggregation concentration was determined for these two monomers as shown in **Figure 4.3a** and **b.** The CAC of **1b** and **2a** was determined from samples prepared in a concentration range from 100 µM to 10 nM. Despite their different UV-vis profiles and solubility in water, **1b** and **2a** displayed comparable CACs ($2.4 \cdot 10^{-5}$ M and $2.13 \cdot 10^{-5}$ M).

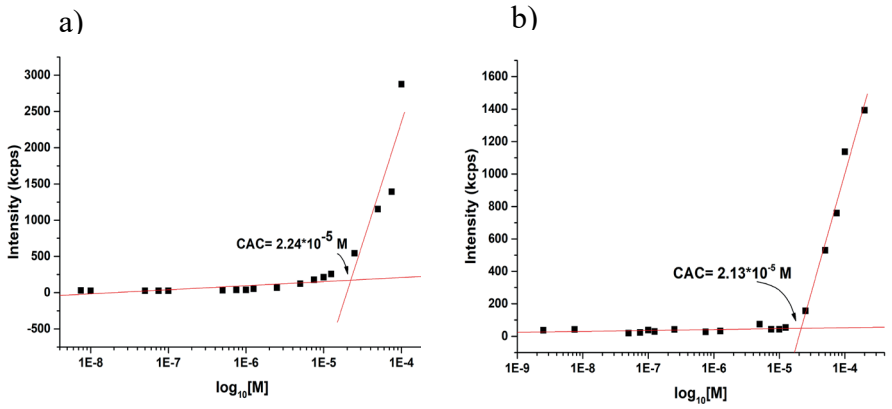


**Figure 4.3** Variable concentration SLS measurement of a) **1b** and b) **2a** to determine the critical aggregation concentration.

To further probe the spectroscopic differences observed in UV-vis measurements that suggest a difference in the aggregation mode of the monomers, AFM imaging was performed to gain insight into the morphology of the aggregates (**Figure 4.4**). Self-assembly of **1b** in water results in the formation of nanofibers consistent with the observed UV-vis spectra (**Figure 4.3a)**. Conversely, the increased hydrophilic character of **2a** resulted in the formation of amorphous structures (**Figure 4.3b**) that could be a drying effect and is consistent with a single absorption band at 280 nm and lack of fluorescent signal in the Nile Red experiment. In case of **2b** and **2c** (**Figure 4.3 c,d**) the formation of fibrillar aggregates is observed with lesser degree of polymerization compared to **1b**. These observed morphologies are in line with the results obtained from UV-vis spectroscopy and point to the importance of the hydrophilic-hydrophobic ratio in combination with the squaramide synthons inside the molecular structure to drive monomer self-assembly into fibrillar aggregates that entangle to form hydrogel materials. To gain further insight into the morphological differences between the aggregates of **1b, 2b** and **2c,** measurements that are performed in the solution state such as small angle x-ray scattering and cryogenic electron microscopy are necessary.

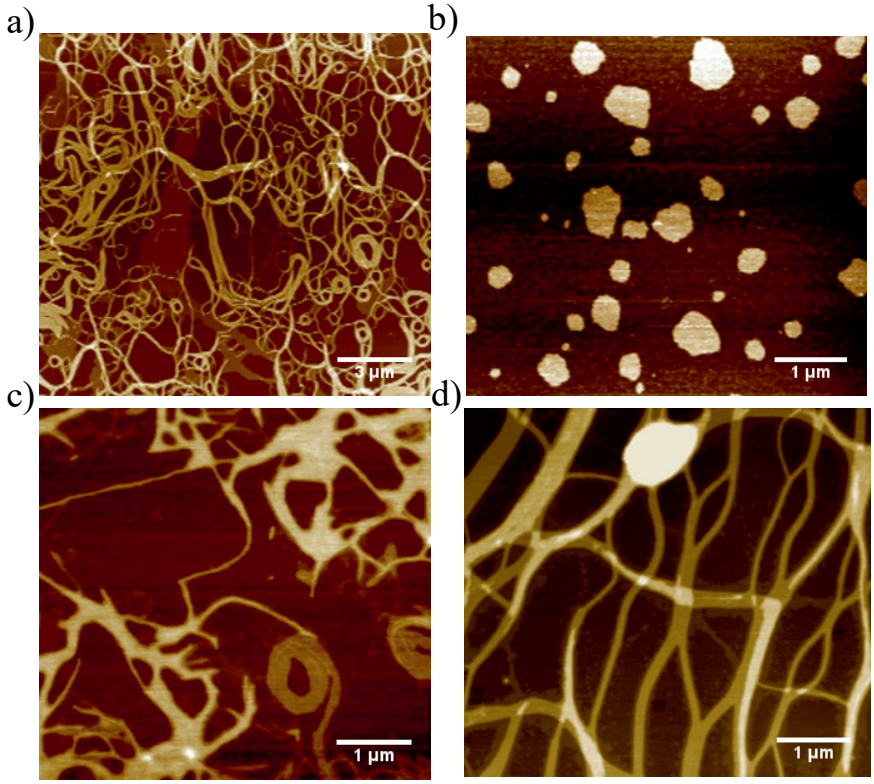


**Figure 4.4** AFM micrographs of **1b (a)** (scale bar 3 µm)**, 2a (b)**, **2b (c)** and **2c (d),** (scale bar: 1 µm).

The capacity of the monomers that form fibrillar aggregates to gelate water were probed by a gel inversion test and oscillatory rheology (**Figure 4.5**). Monomers **2b** and **2c** did not yield hydrogels, as they precipitated at a higher concentration of 1 mM likely due to their increased hydrophobic character in comparison to the other monomers. Alternatively, **1b** gelated water. In contrast to gelator **1a** that showed a cgc at 3.1 mM, **1b** exhibited higher cgc of 5 mM and viscous solutions at lower concentrations. The stiffness of the hydrogel composed of **1b** was further quantified by oscillatory rheology in a time sweep measurement. The storage modulus (G') at the end of the measurement was 16 Pa. This value is lower in comparison to the G' obtained for **1b** (67 Pa) in a similar concentration range.

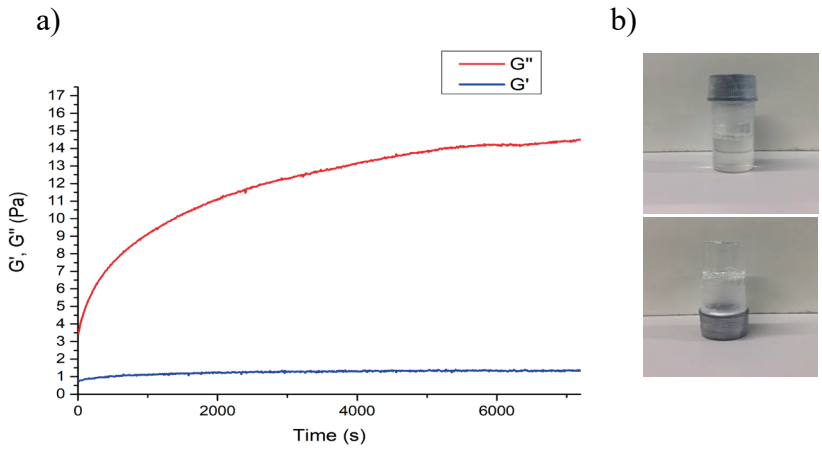


**Figure 4.5** (a) Oscillatory rheology time sweep of **1b**, ($c_{SQ}$=5 mM), Time sweep measurements were collected at a fixed frequency of 1.0 Hz and strain of 0.05% for up to 7200s. (b) Representative photograph of the gel inversion test for **1b** at 5 mM.

Overall, the structural modifications to monomers **1b** and **2a-c** and their self-assembly demonstrated the extent they could be altered while preserving supramolecular polymer assembly. Maintenance of a sufficient hydrophilic/hydrophobic ratio despite a reduction of one squaramide unit in **2b, 2c** permitted the formation of supramolecular polymers, however gel phase materials are not obtained. More specifically, removal of the hydrophobic domain at the core in **2a** results in loss of nanofiber formation as evidenced by spectroscopic and AFM measurements. Retention of a hydrophobic domain at the core with and without oligoethyelene glycol as in **2b** and **2c** provides nanofibers with increased flexibility and a lesser degree of polymerization compared to **1b**. Moreover, in these experiments the carbamate moiety in **1** was found to be relevant for increasing hydrogel stiffness. In the absence of the carbamate a four-fold lower storage modulus of the hydrogel was obtained.

## 4.4 Conclusions

In this study, the systematic modification of the chemical structure of tripodal squaramide monomer on their self-assembly properties was examined in water. Thus, a small library of monomers was synthesized in moderate yields and their self-assembly properties were investigated and compared with the corresponding parental tripodal squaramide-based hydrogelator. Exchange of the carbamates with the ether linkages resulted in a reduction in hydrogel stiffness, whereas reduction of the number of squaramide units resulted inability to form gel phase materials. The observed effects on gelation likely result due to the reduced degrees of polymerization of the squaramide monomers with a reduction in the number of the squaramide synthons affecting their entanglement. Additionally, the hydrophobic shielding of the regions near squaramide are critical as an increase in hydrophilicity near the center of the monomer hinders the formation of fibrillar aggregates. These results point to the importance of the location of the hydrophilic moieties on the self-assembly of the aggregates, and the hydrophilic/hydrophobic ratio. Cumulatively, these demonstrate the necessary structural features to guide the gelation of tripodal squaramide-based monomers in solution, but also their hints at their tolerance to structural modifications for future works that involve their conversion into functional supramolecular biomaterials.

## References


1. Aida, T.; Meijer, E. W.; Stupp, S. I., Functional Supramolecular Polymers. *Science* **2012,** *335*, 813-817
2. Yang, L.; Tan, X.; Wang, Z.; Zhang, X., Supramolecular polymers: historical development, preparation, characterization, and functions. *Chem. Rev.* **2015,** *115*, 7196-7239.
3. Webber, M. J.; Appel, E. A.; Meijer, E. W.; Langer, R., Supramolecular biomaterials. *Nat. Mater.* **2016,** *15*, 13-26.
4. El-Sherbiny, I. M.; Yacoub, M. H., Hydrogel scaffolds for tissue engineering: Progress and challenges. *Glob. Cardiol. Sci. Pract.* **2013,** *2013*, 316-42.
5. Guan, X.; Avci-Adali, M.; Alarcin, E.; Cheng, H.; Kashaf, S. S.; Li, Y.; Chawla, A.; Jang, H. L.; Khademhosseini, A., Development of hydrogels for regenerative engineering. *Biotechnol. J.* **2017,** *12*, 1-19.
6. Larraneta, E.; Stewart, S.; Ervine, M.; Al-Kasasbeh, R.; Donnelly, R. F., Hydrogels for Hydrophobic Drug Delivery. Classification, synthesis and Applications. *J. Funct. Biomater.* **2018,** *9*, 1-20.
7. Geckil, H.; Xu, F.; Zhang, X.; Moon, S.; Demirci, U., Engineering hydrogels as extracellular matrix mimics. *Nanomedicine (Lond)* **2010,** *5*, 469-484.
8. Rosales, A. M.; Anseth, K. S., The design of reversible hydrogels to capture extracellular matrix dynamics. *Nat. Rev. Mater.* **2016,** *1*, 1-15.
9. Eichstaedt, K.; Szpotkowski, K.; Grajda, M.; Gilski, M.; Wosicki, S.; Jaskólski, M.; Szumna, A., Self-Assembly and Ordering of peptide-based cavitands in water and DMSO: The power of hydrophobic effects combined with neutral hydrogen bonds. *Chem. Eur. J.* **2019,** *25*, 3091-3097.
10. Besenius, P.; Portale, G.; Bomans, P. H. H.; Janssen, H. M.; Palmans, A. R. A.; Meijer, E. W., Controlling the growth and shape of chiral supramolecular polymers in water. *Proc. Natl. Acad. Sci.* **2010,** *107*, 17888-17893.
11. Cantekin, S.; de Greef, T. F. A.; Palmans, A. R. A., Benzene-1,3,5-tricarboxamide: a versatile ordering moiety for supramolecular chemistry. *Chem. Soc. Rev.* **2012,** *41*, 6125-6137.
12. Cui, H.; Webber, M. J.; Stupp, S. I., Self-assembly of peptide amphiphiles: from molecules to nanostructures to biomaterials. *Biopolymers* **2010,** *94*, 1-18.
13. Hendricks, M. P.; Sato, K.; Palmer, L. C.; Stupp, S. I., Supramolecular assembly of peptide amphiphiles. *Acc. Chem. Res.* **2017,** *50*, 2440-2448.

14. Dankers, P. Y. W.; Hermans, T. M.; Baughman, T. W.; Kamikawa, Y.; Kieltyka, R. E.; Bastings, M. M. C.; Janssen, H. M.; Sommerdijk, N. A. J. M.; Larsen, A.; van Luyn, M. J. A.; Bosman, A. W.; Popa, E. R.; Fytas, G.; Meijer, E. W., Hierarchical formation of supramolecular transient networks in water: a modular injectable delivery system. *Adv. Mat.* **2012,** *24*, 2703-2709.
15. Ramaekers, M.; de Feijter, I.; Bomans, P. H. H.; Sommerdijk, N. A. J. M.; Dankers, P. Y. W.; Meijer, E. W., Self-Assembly of chiral supramolecular ureido-pyrimidinone-based poly(ethylene glycol) polymers via Multiple Pathways. *Macromolecules* **2014,** *47*, 3823-3828.
16. Nieuwenhuizen, M. M. L.; de Greef, T. F. A.; van der Bruggen, R. L. J.; Paulusse, J. M. J.; Appel, W. P. J.; Smulders, M. M. J.; Sijbesma, R. P.; Meijer, E. W., Self-Assembly of ureido-pyrimidinone dimers into one-dimensional stacks by lateral hydrogen bonding. *Chem. Eur. J.* **2010,** *16*, 1601-1612.
17. Long, K.; Liu, Y.; Li, Y.; Wang, W., Self-assembly of trigonal building blocks into nanostructures: molecular design and biomedical applications. *J. Mat. Chem. B* **2020,** *8*, 6739-6752.
18. Gibson, S. E.; Castaldi, M. P., C3 symmetry: molecular design inspired by nature. *Angew. Chem. Int. Ed. Engl.* **2006,** *45*, 4718-4720.
19. Dorca, Y.; Matern, J.; Fernández, G.; Sánchez, L., $C_3$-Symmetrical π-scaffolds: useful building blocks to construct helical supramolecular polymers. *Isr. J. Chem.* **2019,** *59*, 869-880.
20. Smulders, M. M. J.; Schenning, A. P. H. J.; Meijer, E. W., Insight into the mechanisms of cooperative self-assembly: The "Sergeants-and-Soldiers" principle of chiral and achiral C3-symmetrical discotic triamides. *J. Am. Chem. Soc.* **2008,** *130*, 606-611.
21. Stals, P. J. M.; Smulders, M. M. J.; Martín-Rapún, R.; Palmans, A. R. A.; Meijer, E. W., Asymmetrically substituted benzene-1,3,5-tricarboxamides: self-Assembly and odd–even effects in the solid state and in dilute solution. *Chem. Eur. J.* **2009,** *15*, 2071-2080.
22. Wang, F.; Gillissen, M. A. J.; Stals, P. J. M.; Palmans, A. R. A.; Meijer, E. W., Hydrogen bonding directed supramolecular polymerisation of oligo(Phenylene-Ethynylene)s: cooperative Mechanism, core symmetry effect and chiral amplification. *Chem. Eur. J.* **2012,** *18*, 11761-11770.
23. Leenders, C. M. A.; Albertazzi, L.; Mes, T.; Koenigs, M. M. E.; Palmans, A. R. A.; Meijer, E. W., Supramolecular polymerization in water harnessing both hydrophobic effects and hydrogen bond formation. *Chem. Comm.* **2013,** *49*, 1963-1965.

24. Leenders, C. M. A.; Baker, M. B.; Pijpers, I. A. B.; Lafleur, R. P. M.; Albertazzi, L.; Palmans, A. R. A.; Meijer, E. W., Supramolecular polymerisation in water; elucidating the role of hydrophobic and hydrogen-bond interactions. *Soft Matter* **2016,** *12*, 2887-2893.
25. Besenius, P.; van den Hout, K. P.; Albers, H. M. H. G.; de Greef, T. F. A.; Olijve, L. L. C.; Hermans, T. M.; de Waal, B. F. M.; Bomans, P. H. H.; Sommerdijk, N. A. J. M.; Portale, G.; Palmans, A. R. A.; van Genderen, M. H. P.; Vekemans, J. A. J. M.; Meijer, E. W., Controlled supramolecular oligomerization of C3-symmetrical molecules in water: the impact of hydrophobic shielding. *Chem. Eur. J.* **2011,** *17*, 5193-5203.
26. Friggeri, A.; van der Pol, C.; van Bommel, K. J. C.; Heeres, A.; Stuart, M. C. A.; Feringa, B. L.; van Esch, J., Cyclohexane-based low molecular weight hydrogelators: a chirality investigation. *Chem. Eur. J.* **2005,** *11*, 5353-5361.
27. van Bommel, K. J. C.; van der Pol, C.; Muizebelt, I.; Friggeri, A.; Heeres, A.; Meetsma, A.; Feringa, B. L.; van Esch, J., Responsive cyclohexane-based low-molecular-weight hydrogelators with modular architecture. *Angew. Chem. Int. Ed.* **2004,** *43*, 1663-1667.
28. Du, X.; Zhou, J.; Shi, J.; Xu, B., Supramolecular hydrogelators and hydrogels: from soft matter to molecular biomaterials. *Chem. Rev.* **2015,** *115*, 13165-13307.
29. Boekhoven, J.; Brizard, A. M.; van Rijn, P.; Stuart, M. C. A.; Eelkema, R.; van Esch, J. H., Programmed morphological transitions of multisegment assemblies by molecular chaperone analogues. *Angew. Chem. Int. Ed.* **2011,** *50*, 12285-12289.
30. Storer, R. I.; Aciro, C.; Jones, L. H., Squaramides: physical properties, synthesis and applications. *Chem. Soc. Rev.* **2011,** *40*, 2330-2246.
31. Wurm, F. R.; Klok, H. A., Be squared: expanding the horizon of squaric acid-mediated conjugations. *Chem. Soc. Rev.* **2013,** *42*, 8220-8236.
32. Marchetti, L. A.; Kumawat, L. K.; Mao, N.; Stephens, J. C.; Elmes, R. B. P., The versatility of squaramides: from supramolecular chemistry to chemical biology. *Chem.* **2019,** *5*, 1398-1485.
33. Saez Talens, V.; Englebienne, P.; Trinh, T. T.; Noteborn, W. E.; Voets, I. K.; Kieltyka, R. E., Aromatic gain in a supramolecular polymer. *Angew. Chem. Int. Ed.* **2015,** *54*, 10502-10506.
34. Zhao, B.-L.; Li, J.-H.; Du, D.-M., Squaramide-catalyzed asymmetric reactions. *Chem. Rec.* **2017,** *17*, 994-1018.

35. Jin, C.; Zhang, M.; Wu, L.; Guan, Y.; Pan, Y.; Jiang, J.; Lin, C.; Wang, L., Squaramide-based tripodal receptors for selective recognition of sulfate anion. *Chem. Commun. (Camb)* **2013,** *49*, 2025-2027.
36. Tong, C.; Liu, T.; Saez Talens, V.; Noteborn, W. E. M.; Sharp, T. H.; Hendrix, M.; Voets, I. K.; Mummery, C. L.; Orlova, V. V.; Kieltyka, R. E., Squaramide-based supramolecular materials for three-dimensional cell culture of human induced pluripotent stem cells and their derivatives. *Biomacromolecules* **2018,** *19*, 1091-1099.
37. Krieg, E.; Bastings, M. M.; Besenius, P.; Rybtchinski, B., Supramolecular Polymers in Aqueous Media. *Chem. Rev.* **2016,** *116*, 2414-2477.
38. Leenders, C. M.; Albertazzi, L.; Mes, T.; Koenigs, M. M.; Palmans, A. R.; Meijer, E. W., Supramolecular polymerization in water harnessing both hydrophobic effects and hydrogen bond formation. *Chem. Commun. (Camb)* **2013,** *49*, 1963-1965.
39. Pandya, D. N.; Pailloux, S.; Tatum, D.; Magda, D.; Wadas, T. J., Di-macrocyclic terephthalamide ligands as chelators for the PET radionuclide zirconium-89. *Chem. Comm.* **2015,** *51*, 2301-2303.
40. Stuart, M. C. A.; van de Pas, J. C.; Engberts, J. B. F. N., The use of Nile Red to monitor the aggregation behavior in ternary surfactant–water–organic solvent systems. *J. Phys. Org. Chem.* **2005,** *18*, 929-934.
41. Topel, Ö.; Çakır, B. A.; Budama, L.; Hoda, N., Determination of critical micelle concentration of polybutadiene-block-poly(ethyleneoxide) diblock copolymer by fluorescence spectroscopy and dynamic light scattering. *J. Mol. Liq.* **2013,** *177*, 40-43.
42. Chirkin, E.; Muthusamy, V.; Mann, P.; Roemer, T.; Nantermet, P. G.; Spiegel, D. A., Neutralization of Pathogenic Fungi with Small-Molecule Immunotherapeutics. *Angew. Chem. Int. Ed* **2017,** *56*, 13036-13040.

# SUPPORTING INFORMATION

## 4.5 Material and methods

### 4.5.1 Materials

All reagents and chemicals were purchased from Sigma Aldrich, Acros Organics and Bioconnect and used without further purification. Deuterated chloroform was purchased from Euriso-top and Milli-Q water was employed for all experiments. Acetonitrile for the hydrogenation reaction was dried using molecular sieves 3Å (20% w/v) and used after 24 h of equilibration. Tetraethylene glycol *p*-toluenesulfonate ($Peg_4OTs$) was synthesized as reported in literature.[42]

### 4.5.2 Instrumentation

Compounds were either purified by normal-phase silica gel column chromatography or on a X1 flash chromatography system equipped with a C18 column from Grace Reveleris. $^{1}$H-NMR and $^{13}$C spectra were obtained on a Bruker (300 MHz) or Bruker DMX-400 (400 MHz). LC-MS analyses were performed on a Finnigan Surveyor HPLC system equipped with a Gemini C18 50 x 4.60 mm column (UV detection at 254 and 214 nm) coupled to Finnigan LCQ Advantage Max mass spectrometer with ESI. For the mobile phase, a gradient of 10-90% of $CH_3CN$/ $H_2O$ with 0.1% trifluoroacetic acid over 13.5 minutes was used. MALDI-TOF-MS spectra were obtained on a Bruker Microflex LRF mass spectrometer in reflection positive mode using α-cyano-4-hydroxycinnamic acid as a matrix with a laser power of 30%. UV-vis measurements were performed on a Cary 300 UV-vis spectrophotometer using a quartz cuvette of a 1 cm path length. DLS measurements were carried out using a Malvern Zetasizer Nano ZS ZEN3500 equipped with a laser of 633 nm and with a scattering angle of 173°. Fluorescence experiments were recorded on an Infinite M1000 Pro Tecan plate reader using a 96-well plate with a black background. Atomic force microscopy (AFM) images were recorded in tapping mode on a Veeco-Bruker Multimode AFM with a Nanoscope IIIa controller at room temperature. The AFM tips used were Oltespa Opus probes with a reflex aluminium coating with a nominal spring constant of 2 N/m, a nominal resonance frequency of 70 kHz and a tip radius of 7 nm. The images were processed using Nanoscope software. The mechanical properties of the squaramide-based hydrogels were measured on a Discovery HR-2 hybrid rheometer using cone-plate geometry (40 mm,

1.995°) at 25 ± 0.2 °C with a Peltier-based temperature controller and a solvent trap.

## 4.6 Synthetic schemes

### 4.6.1 Synthethic procedure 1: Squaramide amphiphile synthesis

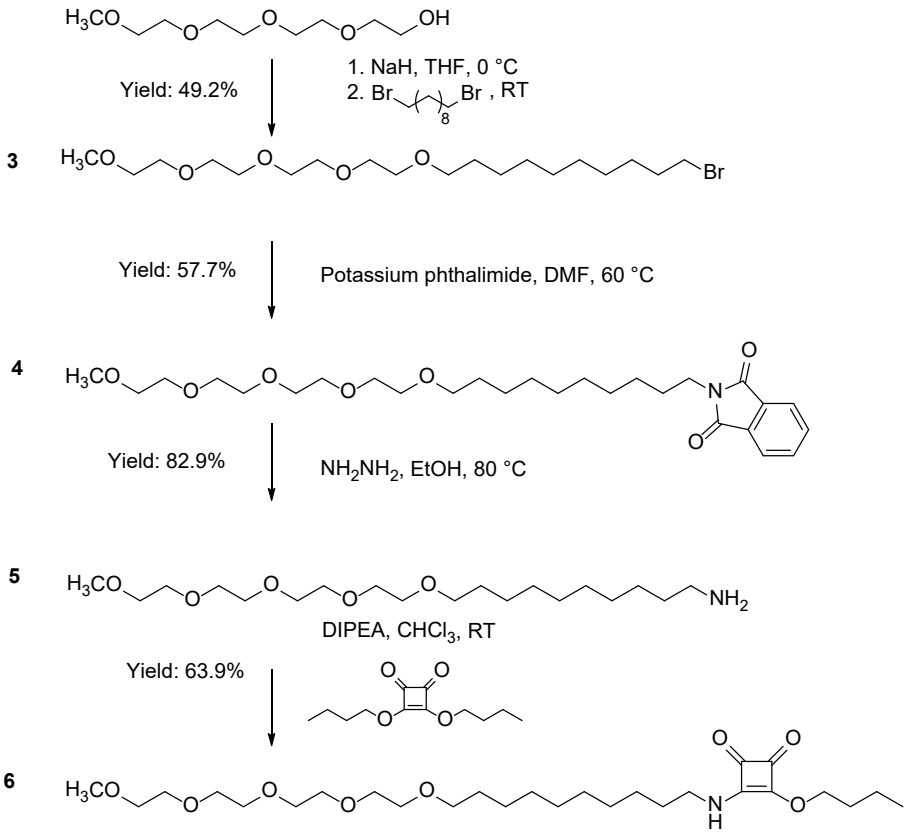

**Synthesis of 3**

Tetraethylene glycol monomethyl ether (3.8 mL, 19.21 mmol) was dissolved in dry THF (20 mL) at 0 ºC. NaH (0.768 g, 19.21 mmol) was added in portions resulting in a foaming solution. When the foaming ceased, the ice bath was removed. Subsequently, 1,10-dibromodecane (12.94 mL, 57.62 mmol) was added and the reaction mixture was stirred overnight at room temperature. The reaction was quenched with $H_2O$ (20 mL) and extracted with diethyl ether (3 x 40 mL). The combined organic fractions were collected, dried with $MgSO_4$, filtered, and concentrated. The product was purified by silica column chromatography (eluent: petroleum ether/EtOAc 8/2-5/5 v/v) and was isolated as a colorless oil.

Yield = 4.04 g, 49.2%. $^1$H NMR (300 MHz, $CDCl_3$): δ (ppm) = 3.58-3.46 (m, 16H), 3.39-3.30 (m, 5H), 1.79-1.72 (t, 2H), 1.52-1.47 (t, 2H), 1.35-1.22 (d, 14H). $^{13}$C NMR (75 MHz, $CDCl_3$): δ (ppm) = 71.87, 71.38, 70.53, 70.45, 70.01, 58.94, 33.87, 33.74, 32.72, 29.56, 29.38, 29.35, 29.29, 28.99, 28.83, 28.66, 28.08, 26.00. TLC-MS (m/z): 450.1 $[M+Na]^+$.

**Synthesis of 4**

**3** (4.04 g, 9.45 mmol) and potassium phthalimide (2.45 g, 13.23 mmol) were dissolved in DMF (15 mL) and the mixture was refluxed for 2 hours. After the removal of the solvent by rotary evaporation, the residue was re-dissolved in DCM (50 mL), extracted with 2 M HCl (2 x 30 mL), dried with $MgSO_4$, filtered, and concentrated. The compound was purified by silica column chromatography (petroleum ether/EtOAc, 1/1) and obtained as colorless oil.

Yield = 2.69 g, 57.7%. $^1$H NMR (300 MHz, $CDCl_3$): δ (ppm) = 7.75 (d, 4H), 3.4 (m, 18H), 3.35 (s, 3H), 1.6 (d, 4H), 1.24 (s, 14H). $^{13}$C NMR (75 MHz, $CDCl_3$): δ (ppm) = 168.40, 133.81, 132.14, 123.10, 71.91, 71.48, 70.57, 70.49, 70.02, 59.00, 38.02, 29.59, 29.46, 29.39, 29.13, 28.56, 26.81, 26.03. TLC-MS (m/z): 516.5 $[M+Na]^+$, 532.5 $[M+K]^+$.

**Synthesis of 5**

Hydrazine monohydrate (3.8 mL, 78.34 mmol) was added to a stirred solution of **4** (2.69 g, 5.45 mmol) in EtOH (50 mL) and the mixture was refluxed overnight. The solvent was removed by rotary evaporation and the mixture was dissolved in chloroform (100 mL), extracted with NaOH (3 x 100 mL, 1 M) and the organic layers were dried with $MgSO_4$, filtered, and concentrated. The compound was isolated as white solid and used for the next step without any further purification.

Yield = 1.64 g, 82.9%. $^1$H NMR (300 MHz, $CDCl_3$): δ (ppm) = 3.40 (m, 16H), 3.26 (t, 2H), 3.20 (s, 3H), 2.50 (t, 2H), 1.80 (s, 3H), 1.30 (m, 4H), 1.11 (s, 12H). $^{13}$C NMR (75 MHz, $CDCl_3$): δ (ppm) = 71.77, 71.28, 70.43, 70.33, 69.90, 58.81, 41.90, 33.31, 29.47, 29.39, 29.37, 29.30, 26.72, 25.92. TLC-MS (m/z): = 364.5 $[M+H]^+$, 386.5 $[M+Na]^+$.

**Synthesis of 6**

**5** (1.18 g, 3.26 mmol), 3,4-dibutoxy-3-cyclobutene-1,2-dione (0.9 mL, 3.91 mmol), and DIPEA (0.9 mL, 4.89 mmol) were dissolved in $CHCl_3$ (50 mL) and were stirred at room temperature for 2 h. The mixture was purified by silica column chromatography (DCM/MeOH, 98/2). The product was isolated as light brown oil.

Yield = 1.07 g, 63.9%. $^1$H NMR (300 MHz, $CDCl_3$): δ (ppm) = 4.73 (t, 2H), 3.66 (m, 16H), 3.43 (t, 4H), 1.77 (q, 2H), 1.56 (m, 4H), 1.44 (m, 2H), 1.27 (s, 12H), 0.96 (t, 3H). $^{13}$C NMR (75 MHz, $CDCl_3$): δ (ppm) = 177.48, 73.38, 71.89, 71.47, 70.58, 70.54, 70.47, 70.02, 59.00, 44.88, 31.99, 30.65, 29.59, 29.44, 29.39, 29.10, 26.34, 26.03, 18.63, 13.65. LC-MS: t = 7.65 min, (m/z): 515.69.$[M]^+$

## 4.6.2 Synthetic procedure 2: Synthesis of 2a, 2b and 2c

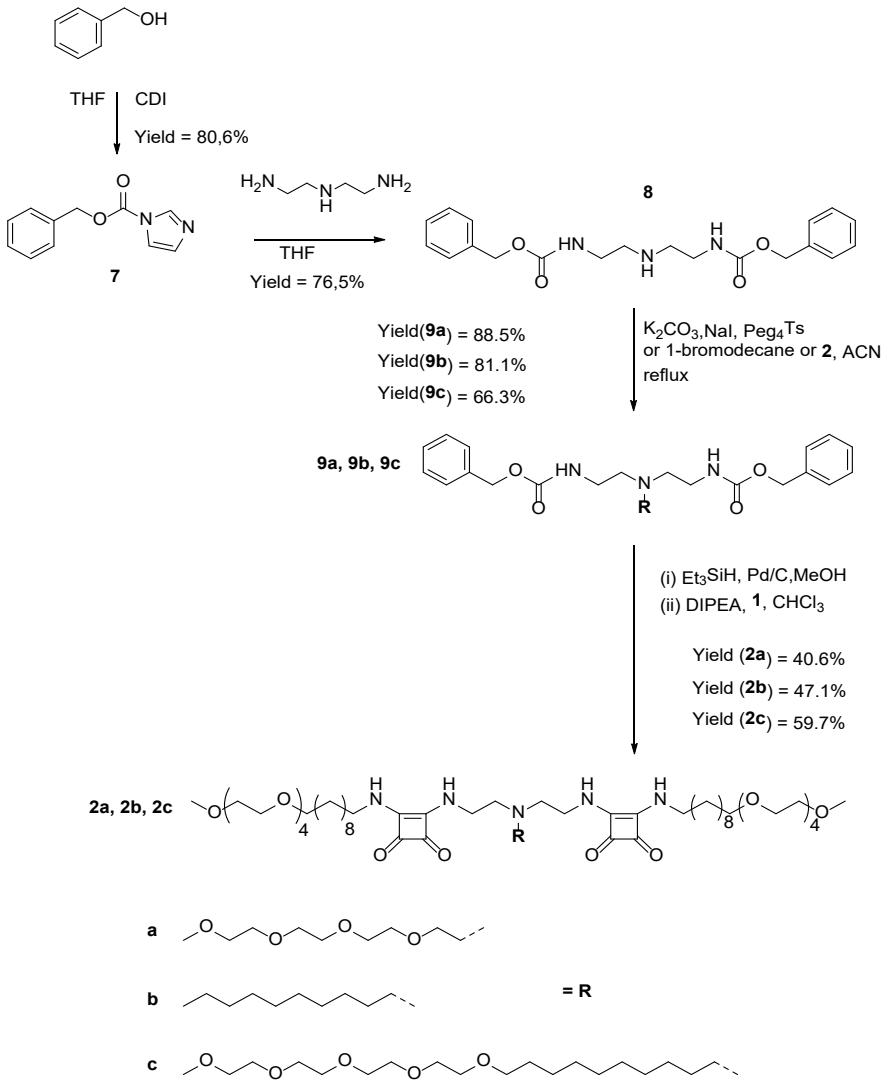

**Synthesis of 7**

Benzyl alcohol (1.6 mL, 15.42 mmol), and CDI (5.00 g, 30.83 mmol) were dissolved in THF (20 mL) and were stirred at RT for 30 minutes under $N_2$ atmosphere. After quenching the reaction with distilled $H_2O$ (70 mL) and extraction with EtOAc (3 x 100 mL), the combined organic fractions were dried with $MgSO_4$, filtered, and concentrated. The solution was purified by silica column chromatography (EtOAc/hexane, 1/2) and the product was isolated as a colorless oil.

Yield = 2.51 g, 80.6%. $^1$H NMR (300 MHz, $CDCl_3$): δ (ppm) = 8.07 (s, 1H), 7.34 (m, 6H), 6.98 (m, 1H), 5.32 (s, 2H). $^{13}$C NMR (75 MHz, $CDCl_3$): δ (ppm) = 148.51, 137.09, 134.02, 130.58, 128.95, 128.78, 128.64, 117.10, 69.73. TLC-MS (m/z): 203.2 $[M+H]^+$, 228.2 $[M+Na]^+$.

**Synthesis of 8**

**7** (2.51 g, 12.41 mmol) was dissolved in THF (50 mL) and diethylenetriamine (0.6 mL, 5.77 mmol) was added dropwise to the reaction mixture and stirred for 2 h at RT. The solution was purified by flash chromatography on a C18 silica column using a gradient of $H_2O/CH_3CN$ 10-90 % over 35 minutes. The product was concentrated and lyophilized.

Yield = 1.64 g, 76.5%. $^1$H NMR (300 MHz, $CDCl_3$): δ (ppm) = 7.33 (s, 10H), 5.65 (t, 2H), 5.08 (s, 4H), 3.25-3.21 (t, 4H), 2.68 (t, 4H), 1.33 (s, 1H). $^{13}$C NMR (300 MHz, $CDCl_3$): δ (ppm) = 156.77, 136.60, 128.50, 128.09, 66.64, 48.59, 40.70. TLC-MS (m/z): 394.3 $[M + Na]^+$.

**Synthesis of 9a**

Tetraethylene glycol *p*-toluenesulfonate (0.42 g, 1.15 mmol), **8** (0.23 g, 0.62 mmol), $K_2CO_3$ (0.12 g, 0.88 mmol), and NaI (0.096 g, 0.64 mmol) were dissolved in anhydrous acetonitrile (15 mL) and were refluxed for 36 hours. The solution was concentrated and the residue was redissolved in DCM (25 mL). After washing with 1 M NaOH (15 mL) and back extraction of the aqueous layers with DCM (3 x 10 mL), the combined organic fractions were dried with $MgSO_4$, filtered, and concentrated. The residue was purified by flash column chromatography on C18 silica column using a gradient of $H_2O/CH_3CN$: 10-90% over 40 minutes.

Yield = 0.31 g, 88.5%. $^{1}$H NMR (300 MHz, $CDCl_3$): δ (ppm) = 7.29 (s, 10H), 5.91 (t, 2H), 5.05 (s, 4H), 3.50 (s, 12H), 3.41 (t, 2H), 3.33 (s, 3H), 3.219 (q, 4H), 2.61 (t, 6H). $^{13}$C NMR (75 MHz, $CDCl_3$): δ (ppm) = 156.80, 136.86, 128.38, 128.05, 127.90, 71.84, 70.49, 70.46, 70.35, 70.32, 70.16, 69.99, 66.39, 58.96, 54.23, 53.19, 39.17.

**Synthesis of 2a**

**9a** (0.149 g, 0.265 mmol) and Pd/C (0.021 g, 0.197 mmol) were dissolved in dry MeOH (10 mL) and placed under a $N_2$ atmosphere. $Et_3SiH$ (4.5 mL, 26.5 mmol) was added dropwise to the reaction mixture and stirred at RT overnight. The solution was filtered over celite and the solvent was removed by a stream of $N_2$ gas. Subsequently, the residue was dissolved in $CHCl_3$ (50 mL) and **6** (0.30 g, 0.59 mmol) and DIPEA (0.14 mL, 0.80 mmol) were added and refluxed overnight. After the removal of the solvent by rotary evaporation, the residue was redissolved in DCM (20 mL), washed with $H_2O$ (3 x 10 mL) and dried with $MgSO_4$, filtered, and concentrated. The final compound was purified by silica column (DCM/MeOH, 9/1), lyophilized and obtained as white solid.

Yield = 0.122 g, 40.6%. $^{1}$H NMR (300 MHz, $CDCl_3$): δ (ppm) = δ 3.59 (m, 50H), 3.42 (t, 8H), 3.35 (s, 6H), 3.31 (s, 3H), 2.68 (m, 6H), 1.58 (m, 12H), 1.24 (s, 20H). $^{13}$C NMR (75 MHz, $CDCl_3$): δ (ppm) = 183.25, 181.50, 168.98, 168.81, 72.26, 71.82, 71.67, 71.49, 70.87, 70.53, 70.49, 70.44, 70.36, 69.92, 58.98, 57.15, 53.89, 44.61, 43.52, 31.14, 29.55, 29.51, 29.44, 29.25, 26.50, 26.03. LC-MS: t= 6.20 min, (m/z): 1175.42 $[M]^+$, MALDI (m/z): 1177.95, $[M+H]^+$

**Synthesis of 9b**

**8** (0.21 g, 0.58 mmol), 1-bromodecane (0.14 mL, 0.67 mmol) and $K_2CO_3$ (0.37 g, 2.69 mmol) were dissolved in dry acetonitrile (30 mL) and refluxed overnight. The compound was purified by silica column chromatography (DCM/MeOH: 95/5).

Yield = 0.24 g, 81.1 %. $^{1}$H NMR (300 MHz, $CDCl_3$): δ (ppm) = 7.32 (s, 10H), 5.08 (s, 2H), 3.23 (t, 4H), 2.48 (m, 6H), 1.27 (d, 16H), 0.91 (t, 3H). $^{13}$C NMR (75 MHz, $CDCl_3$): δ (ppm) = 156.68, 136.72, 128.44, 128.01, 127.98, 66.56, 54.03, 53.51, 38.86, 34.01, 31.93, 31.90, 29.71, 29.62, 29.53, 29.36, 29.30, 27.39, 26.89, 22.71, 14.16. TLC-MS (m/z): 512.7 $[M + H]^+$, 534.7 $[M + Na]^+$.

**Synthesis of 2b**

**9b** (0.71 g, 1.39 mmol) and Pd/C (0.08 g, 0.72 mmol) were dissolved in dry MeOH (30 mL) and flushed with argon for 10 minutes. $Et_3SiH$ (11.0 mL, 68.9 mmol) was added dropwise to the reaction mixture and stirred overnight at RT. The solution was filtered over celite and the solvent was removed by a stream of $N_2$ gas. Subsequently, the residue was redissolved in $CHCl_3$ (50 mL) and **6** (0.32 g, 0.61 mmol) and DIPEA (0.17 mL, 0.99 mmol) were added and refluxed overnight. After the removal of the solvent by rotary evaporation, the mixture was dissolved in DCM (20 mL) and washed with $H_2O$ (3 x 10 mL) and dried with $MgSO_4$. The product was purified silica column chromatography using DCM/MeOH (9:1) and successively lyophilized to obtain the final compound as a white powder.

Yield = 0.17 g, 47.1%. $^{1}$H NMR (300 MHz, $CDCl_3$): δ (ppm) = δ 3.65 (m, 35H), 3.44 (t, 4H), 3.38 (s, 5H), 2.73 (t, 6H), 1.59 (m, 12H), 1.25 (d, 36H), 0.88 (m, 3H). $^{13}$C NMR (75 MHz, $CDCl_3$): δ (ppm) = 181.81, 168.79, 167.18, 71.85, 71.53, 70.57, 70.53, 70.46, 70.38, 70.01, 69.94, 59.01, 57.41, 54.76, 44.68, 31.91, 31.07, 29.63, 29.59, 29.54, 29.50, 29.35, 29.29, 26.57, 26.07, 22.68, 14.13. LC-MS: t= 8.06 min, (m/z): 1125.62 $[M]^+$), MALDI (m/z): 1127.23 $[M+H]^+$.

**Synthesis of 9c**

**8** (0.20 g, 0.54 mmol) and **3** (0.29 g, 0.67 mmol) and $K_2CO_3$ (0.37 g) were dissolved in dry acetonitrile (30 mL) and refluxed overnight. The purification was performed by flash chromatography on a C18 silica column using a gradient of $H_2O/CH_3CN$ (10-90%) over 40 min.

Yield = 0.26 g, 66.3 %. $^{1}$H NMR (300 MHz, $CDCl_3$): δ (ppm) = 7.33 (d, 10H), 5.08 (s, 4H), 3.66 (m, 17H), 3.57 (m, 4H), 3.45 (m, 3H), 3.39 (d, 3H), 3.26 (s, 2H), 2.52 (d, 4H), 1.58 (t, 3H), 1.27 (d, 16H). $^{13}$C NMR (75 MHz, $CDCl_3$): δ (ppm) = 136.61, 128.45, 128.02, 71.93, 71.52, 70.61, 70.59, 70.51, 70.05, 66.63, 54.06, 53.55, 29.63, 29.55, 29.46, 27.30, 26.08.

**Synthesis 2c**

**7c** (0.18 g, 0.25 mmol), and Pd/C (13 mg, 0.13 mmol) were dissolved in MeOH (30 mL) and flushed with $N_2$ gas for 10 minutes. $Et_3SiH$ (4.0 mL, 25.21 mmol) was added dropwise and the reaction mixture stirred overnight at RT. The solution was filtered over celite and concentrated using a gentle stream of $N_2$ gas. Subsequently, the residue, **6** (0.44 g, 0.85 mmol) and DIPEA (0.19 mL, 1.10 mmol) were dissolved in chloroform and refluxed overnight. After the removal of the solvent, the residue was dissolved in DCM (20 mL), washed (3 x 10 mL) with $H_2O$ and dried with $MgSO_4$. The compound was purified by silica column chromatography using EtOAc and then DCM/MeOH (9/1). Successively, the final compound was lyophilized and isolated as a white powder.

Yield = 0.11 g, 21.5%. $^{1}$H NMR (300 MHz, $CDCl_3$): δ (ppm) = 3.58 (m, 54H), 3.45 (m, 8H), 3.37 (s, 9H), 2.56 (d, 6H), 1.40 (m, 46H). $^{13}$C NMR (75 MHz, $CDCl_3$): δ (ppm) = 185.16, 168.71, 167.27, 71.89, 71.85, 71.53, 70.56, 70.52, 70.44, 70.37, 70.02, 69.92, 69.56, 59.01, 44.59, 37.71, 31.08, 26.54, 26.06. LC-MS: t= 7.14 min, (m/z): 1331.65$[M]^+$, MALDI (m/z): 1355.31 $[M+Na+H]^+$.

### 4.6.3 Synthetic procedure 3: Synthesis of 1b

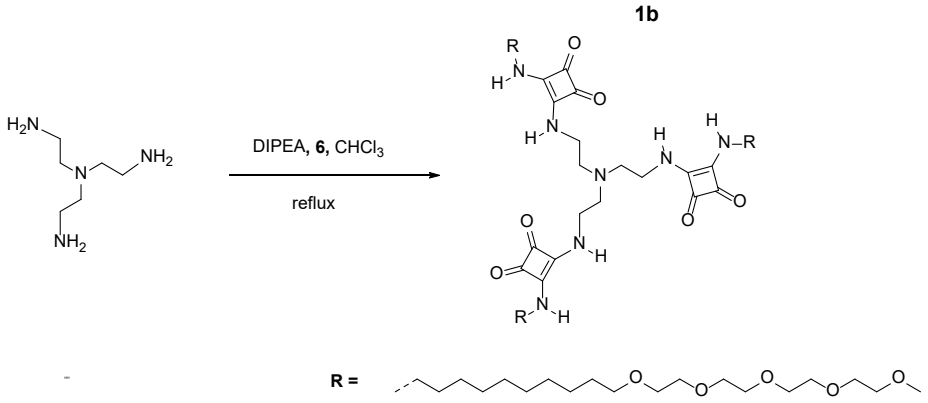


**Synthesis of 1b**

Tris(2-aminoethyl)amine (0.015 mL, 0.10 mmol), **6** (0.17 g, 0.34 mmol) and DIPEA (0.071 mL, 0.05 mmol) were dissolved in chloroform (50 mL) and refluxed overnight. The solvent was removed by rotary evaporation and the residue was dissolved in DCM (15 mL), washed with $H_2O$ (3 x 10 mL) and dried with $MgSO_4$. The compound was purified by silica column chromatography using EtOAc and then DCM/MeOH (9/1) to isolate the product was isolated as a colourless oil.

Yield = 0.131 g, 86.9%. $^{1}$H NMR (300 MHz, $CDCl_3$): δ (ppm) = 7.65 (s, 4H), 3.60 (m, 60H), 3.45 (t, 6H), 3.38 (d, 9H), 2.62 (s, 4H), 1.57 (m, 12H), 1.35 (d, 6H), 1.25 (s, 30H). $^{13}$C NMR (75 MHz, $CDCl_3$): δ (ppm) = 182.66, 168.50, 167.17, 71.66, 71.52, 70.31, 70.19, 70.16, 70.11, 70.04, 69.71, 59.01, 56.69, 55.65, 44.50, 31.08, 29.51, 29.44, 29.24, 26.46, 25.96. LC-MS: t= 6.99 min, (m/z): 1469.83 $[M]^+$), MALDI (m/z): 1470.87 $[M+H]^+$.

## 4.7 Characterization

### Sample preparation protocol

Water was added to **1b** and **2a-c** to prepare solutions at a concentration of 1 mM - 5 mM and sonicated for 20 min using a Branson 2510 Ultrasonic cleaner bath. Subsequently, aliquots from the stock solution were taken to prepare solutions at the desired concentration for solution phase measurements and used for gelation experiments. All samples were left to stand overnight before measurement.

### UV-vis spectroscopy

Samples for UV-vis spectroscopy were prepared at a 15 μM concentration in water as described according to the sample preparation protocol above. The samples were placed in the UV-vis and a spectrum was recorded from 200-500 nm. The solutions were prepared in triplicate and for each solution the UV-vis spectra was measured.

### Fluorescence spectroscopy

A stock solution of Nile Red dye (0.005 mg/mL) was prepared in MeOH. The stock solution was pipetted into 4 individual wells of a 96-well plate (12 μL) and the solvent was removed using a vacuum oven for 2 h. Subsequently **2a, 2b, 2c** and **1a** were prepared at a 15 μM concentration as described according to the self-assembly protocol. Aliquots of **1a** and **2a-c** (200 μL) were pipetted into a 96-well plate and equilibrated overnight before the measurement. Water (200 μL) was measured as a negative control. The experiment was performed using Infinite M1000 Pro Tecan plate reader, with an excitation wavelength of 550 nm and measuring fluorescence emission from 570 to 800 nm. The solutions were prepared in triplicate and for each solution the emission spectra was measured.

### Critical aggregation concentration determination

The critical aggregation concentration (CAC) of **1b** and **2a** was determined by first preparing a stock solution at 1 mM concentration that was equilibrated overnight. The stock solution was diluted to several concentrations between 100 μM to 10 nM and equilibrated for at least 3h prior to measurement of

scattering intensity. Each measurement was carried out using a disposable DLS cuvette. The data was plotted using the scattering intensity as a function of log [C]. The critical aggregation concentration was then determined from the intersection of the two lines drawn through the points collected for the scattering intensities collected at the various concentrations.

**Atomic force microscopy (AFM)**

**1b** and **2a-c** were prepared according to the preparation protocol above at a concentration of 15 μM and equilibrated overnight. An aliquot (25 μL) from each of these solutions was pipetted on cleaved mica and dried overnight at RT before the measurements. The analysis of AFM images was performed using the Nanoscope software.

**Critical gelation concentration (CGC)**

The CGC of compounds **1b** and **2a-c** was determined by the gel inversion method. Compounds **1b** and **2a-c** were weighed in the appropriate quantities in 500 μL of water to prepare gels with final gelator concentrations from 1-5 mM according to the sample preparation protocol above.

**Oscillatory rheology**

Because compound **1a** resulted in a viscous solution at a concentration of 5 mM in water after sonication, an oscillatory rheology measurement was performed to gain insight into the gel properties. The pre-made hydrogel (600 μL) was gently pipetted onto the lower plate and a gap distance was set at 54 μm. Time sweep measurements were collected at a fixed frequency of 1.0 Hz and strain of 0.05% for up to 7200s.

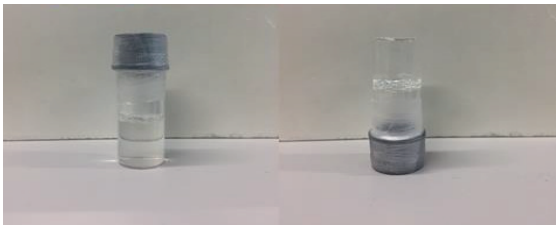

**Figure S1** Representative photograph of gel inversion test for **1b** at 5 mM.

**Table S1**
**TEG weight fraction ($\omega_{TEG}$) of the monomers**

| **Monomers** | $\omega_{TEG}$ |
|---|---|
| **1a** | 0.42 |
| **2a** | 0.55 |
| **2b** | 0.53 |
| **2c** | 0.46 |

## References

1. Chirkin, E.; Muthusamy, V.; Mann, P.; Roemer, T.; Nantermet, P. G.; Spiegel, D. A., Neutralization of Pathogenic Fungi with Small-Molecule Immunotherapeutics. *Angew. Chem. Int. Ed.* **2017,** *56*, 13036-13040.